Pulse-field Actuation of Collinear Magnetic Single Crystals

by

Catherine A. Jenkins

Submitted to the Department of Materials Science and Engineering
in partial fulfillment of the requirements for the degree of

Bachelor of Science in Materials Science and Engineering

at the

MASSACHUSETTS INSTITUTE OF TECHNOLOGY

[February 2004]
December 2003

Author .....
Department of Materials Science and Engineering
May 22, 2003

Certified by .....
Samuel M. Allen
POSCO Professor of Physical Metallurgy
Thesis Supervisor

Certified by .....
Robert C. O'Handley
Senior Research Associate
Thesis Supervisor

Accepted by .....
Caroline A Ross
Chair, Undergraduate Thesis Committee

Pulse-field Actuation of Collinear Magnetic Single Crystals

by

Catherine A. Jenkins

Submitted to the Department of Materials Science and Engineering
on May 22, 2003, in partial fulfillment of the
requirements for the degree of
Bachelor of Science in Materials Science and Engineering

Abstract

Ferromagnetic shape memory alloys (FSMAs) are a class of alloys that exhibits the shape memory effect, as in the alloy nickel–titanium, sometimes known as Nitinol. In FSMAs, though, the shape changes are not brought on just by changes in temperature or mechanical stresses, but can also be driven by the application of a relatively small magnetic field. The large strains exhibited by such materials are a result of the coexistence of several features, including a thermoelastic martensitic transition, and a ferromagnetic martensite (non-equilibrium, low-temperature) phase. The magnetocrystalline anisotropy must also be large, as seen in similar alloys such as iron–palladium ($Fe_{70}Pd_{30}$) [1].

Nickel–manganese–gallium is an FSMA that has shown up to 10% strain in certain orientations as an effect of unconstrained magnetic actuation [4]. To achieve cyclic actuation in FSMAs, the field-induced extension has conventionally been reversed by a compressive mechanical stress from a spring or field orthogonal to the actuating field. The use of a second FSMA crystal to provide the reset force was unreported. Collinear single crystals are shown here to be able to induce a 2.8% reset strain against one another when subjected alternately to individual pulsed magnetic fields in a custom designed and constructed apparatus. A setup of this type could be used in a bistable microswitch, linear motion actuator, or shutter controller where a low actuation stress is sufficient or the electrical contacts required to activate a piezoelectric device are undesirable.

Thesis Supervisor: Samuel M. Allen
Title: POSCO Professor of Physical Metallurgy

Thesis Supervisor: Robert C. O'Handley
Title: Senior Research Associate

Acknowledgments

Grateful acknowledgement is due for the long-suffering assistance of Jorge Feuchtwanger, Robin Ivester, Bob O'Handley, and Sam Allen for generally making the lab a pleasant place to be for more than two years. David Bono's help with the circuitry is appreciated, as is the wit and occasional useful comment from Zil 'Harvard' Lyons, Miguel 'It's Not A Coconut' Marioni, Marc Richard(s), and Bradley William Peterson. Heartfelt thanks also to Fred Cote for telling me off on a regular basis and to Yinlin Xie and the rest of the group for technical advice and assistance.

Uncountably infinite thanks to my parents Liz and Philip, for whom there are no words. To TommyZCat Rozzi, whose fault it is that I am here at all. This entire production was brought to you by Thursdays and the letter five.

Contents

1 Introduction **13**

1.1 Background 13

1.2 Motivation 14

2 Experimental Procedure **17**

2.1 Crystal Preparation 17

2.2 Custom Apparatus Design 18

3 Results **21**

3.1 Crystal Characterization 21

3.1.1 Torque Magnetometry 21

3.1.2 Vibrating Sample Magnetometry 22

3.1.3 Resistance 24

3.2 Pulse-Field Testing 24

3.2.1 Apparatus Improvements 24

4 Discussion **27**

5 Conclusions and Future Work **29**

List of Figures

1-1 Shown is a representative plot of the stress-strain curve of an active FSMA. A large blocking stress is desirable, as well as a low c_{tb} 14

1-2 High magnetocrystalline anisotropy means that it is a more favorable process to restructure the crystal lattice in response to a magnetic field than it is to reorient the magnetizations. The application of an external field causes a 6% change (depending on the c/a ratio and other factors) in the length of the c-axis between the stable tetragonal orientations orthogonal to each other. Adapted from [10]. 15

2-1 Experimental setup of pulse-field apparatus. One crystal is initially compressed and the other fully elongated so that when the first crystal is subjected to the magnetic field the growth in volume fraction of the favored variant will result in a macroscopic elongation of the entire sample. 18

3-1 Torque magnetometry data from a representative laminate crystal. The applied field of 100 Oe was assumed to be too weak to decouple the magnetization M from the c-axis of the crystal lattice. 23

3-2 VSM plot of magnetization versus temperature showing T_M and T_C. T_M is where the magnetization rises sharply with a slight temperature increase as austenite grows to be the primary phase. T_C is the temperature at which the magnetic moments are no longer as strongly aligned, resulting in a decrease in magnetization. 23

-1 Schematic of dual circuit for capacitor-driven field actuation 32

List of Tables

3.1 Resistance R was measured with the sensor leads of the four-point setup separated by a distance L =2.59 mm. Orientation is quoted with respect to the magnetic easy axis of the primary variant relative to the applied current direction. Resistivity ρ was calculated using the measured cross-sectional area: $\rho = \frac{RA_{XS}}{L}$. 25

3.2 The maximum repeatable reset strain exhibited is 1.4% on each laminate sample, due to a combination of a lossy apparatus and skewed endfaces, resulting in unevenly transferred stresses from the extension of the crystals. 25

3.3 The TL8 samples showed a maximum reset strain of 2.8%, or a total change in length of 0.38 mm. The improvement is likely a result of an improved force transferrence centerpiece and a more compact cross-sectional geometry in the cut crystals. 25

Chapter 1

Introduction

Active materials such as piezoelectric materials and shape-memory alloys exhibit a shape change in response to an applied stimulus such as a temperature change or electrical voltage. Common alloys like stoichiometric nickel-titanium are used in biomedical applications such as arterial stents, and the piezoelectric lead-zirconate-titanate is used in everything from driving ultrasonic cell penetration to the nanopositioning of laser mirrors. Naval and other defense applications of active materials include sonar transducers and trigger release mechanisms.

1.1 Background

Ferromagnetic shape memory alloys (FSMAs) are a class of active materials discovered in 1992 that tend to show a much greater strain than comparably processable piezoelectrics. Iron–palladium and off-stoichiometric nickel–manganese–gallium are studied for their large theoretical strains and low threshold blocking field, with the intent of developing applications such as linear motion actuators. Ni_2MnGa had been previously known as a shape-memory alloy but its field-induced actuation was only seen in 1996. Single crystals of Ni–Mn–Ga have been studied since that time when Ukrainian researchers first produced active crystals. Carefully treated, relatively defect-free samples can respond to small (4.2 kOe) magnetic fields with an elongation of up to 6% in tetragonal and 10% in orthorhombic martensites [4].

The mechanism for such large magnetically-induced shape changes is not the same as in magnetostrictive materials such as elemental nickel or Terfenol-D. Instead, a phase-transformationless reorientation of the tetragonal unit cells in the FSMA crystal aligns the axis of easy magnetization with the applied field by moving crystal imperfections known as twin boundaries. These twin boundaries are planes along which the distorted tetragonal lattice has pseudomirror symmetry.

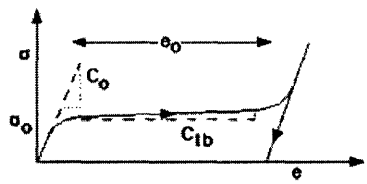

Figure 1-1: Shown is a representative plot of the stress-strain curve of an active FSMA. A large blocking stress is desirable, as well as a low c_{tb}

Because the magnetocrystalline anisotropy of the Heusler alloy Ni_2MnGa is high, single crystals respond to applied magnetic fields by restructuring the unit cell to be oriented with the c-axis parallel to the field, rather than simply responding magnetically and rotating the magnetization to lower the energy of the system. This response also, by necessity, preserves the continuity of the magnetic moments across the boundary.

The increase in volume fraction of the favored variant decreases the magnetic energy $-\vec{H} \cdot \vec{M}$ of the crystal more than a simple rotation of the magnetization would [2, 3]. If the elongation is carefully controlled, there is then excess field energy that can be converted to mechanical work.

1.2 Motivation

Based on the assumption that excess field energy can be converted directly to a mechanical driving force and the knowledge that magnetic energy per unit volume is dimensionally equivalent to a mechanical stress multiplied by strain, an apparatus was designed with two crystals of Ni_2MnGa. Each sample was centered in its own individual Helmholtz coil, with an acrylic spacer placed between each sample to min-

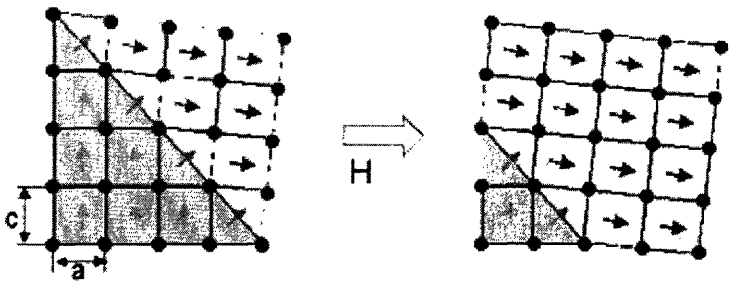

Figure 1-2: High magnetocrystalline anisotropy means that it is a more favorable process to restructure the crystal lattice in response to a magnetic field than it is to reorient the magnetizations. The application of an external field causes a 6% change (depending on the c/a ratio and other factors) in the length of the c-axis between the stable tetragonal orientations orthogonal to each other. Adapted from [10].

imize field crosscoupling, and actuated alternately to prove the feasibility of such a two-crystal setup.

The advantages of FSMA crystals in place of piezo ceramic actuators include the fact that magnetic fields can act without direct physical contact. Also, classic shape memory alloys are actuated by a temperature gradient, severely limiting their frequency response. The local strain of over 6% is also significantly greater than even the best piezo device, which exhibits strains on the order of 0.2%. Also, Joule heating of the electrically coupled device is avoided by removing any need for physical coupling, compensating for the eddy-current heating of the highly resistive single crystals [9]. Twin boundary motion is a highly dissipative process and is being further explored as a mechanism for vibration damping. The inherent lossiness of twin boundary motion also reduces the likelihood of overshoot in a two-crystal setup, with the compression of one crystal damping the extension of the other. In addition, a motor device based on actuator materials rather than mechanical pistons has the advantage of not having moving parts in the system.

The composition of Ni–Mn–Ga has a large effect on any possible field-induced strain, and crystals here were carefully chosen to express a martensitic transition and Curie temperature well above the operating temperature. In future experiments it may be desirable to monitor the compositional and second-phase homogeneity of the crystals even more carefully due to this dependence.

Chapter 2

Experimental Procedure

In this chapter are recorded the setup conditions of each analytical experiment as well as the test procedures using the custom-built apparatus.

2.1 Crystal Preparation

For initial trials, single crystal laminates of about 0.1 x 1.0 x 2.0cm were grown and heat treated at Adaptamat, Inc., exhibiting on average 5.3% strain in response to a threshold field of 3.3 kGa.

For later experiments, the samples were cut from bulk single crystals obtained from T.A. Lograsso at Ames National Laboratory in Ames, Iowa. Crystalline prisms measuring approximately 0.5 x 0.5 x 2.1cm were spark cut at around 40° from the boule axis in order to expose faces along {100}. The end faces were then spark eroded with a 90V arc to be parallel, and then polished down to 0.06μm alumina. Any cutting scraps were ground for compositional and structural analysis by x-ray diffraction.

In order to transform the as-grown austenitic crystals to an active martensite variant, the polished samples were wrapped in tungsten wire and encapsulated in a quartz tube backfilled with argon, with a tantalum getter. They were then heated at 800°C for 24 hours in a Lindberg Model 51333 furnace, cooled to 500°C for four hours to chemically order the sample, and held at 200°C for eight hours. The samples were

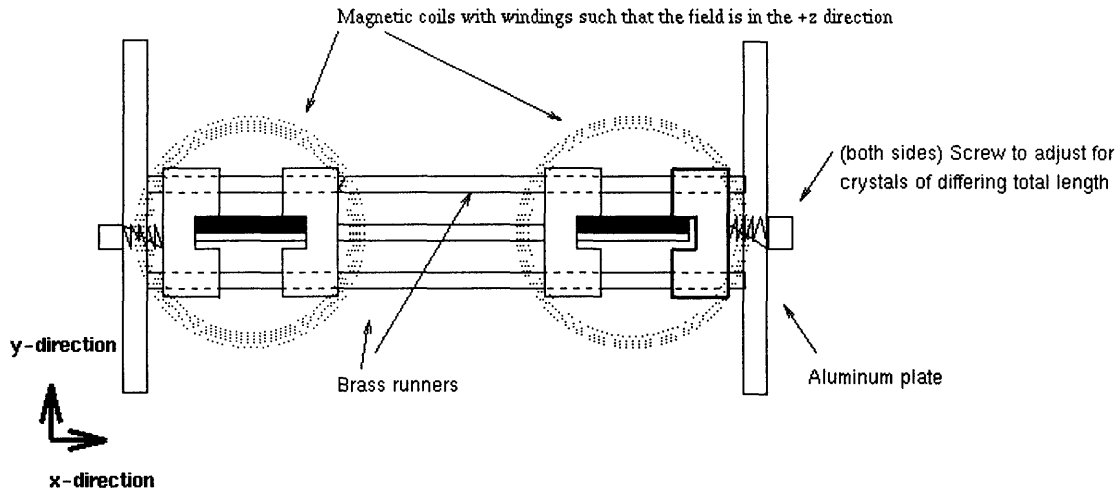

Figure 2-1: Experimental setup of pulse-field apparatus. One crystal is initially compressed and the other fully elongated so that when the first crystal is subjected to the magnetic field the growth in volume fraction of the favored variant will result in a macroscopic elongation of the entire sample.

then removed from the furnace, the tubes broken, the wrapping wires cut, and the samples held under 30lbs (135 N) compressive force at zero field while cooling past the martensitic transition (T_M) to room temperature.

Magnetization versus temperature curves over the range of 0 C to 80 C at 500 Oe were taken using a vibrating sample magnetometer. Strains for the TL8 samples were about 5.0%.

2.2 Custom Apparatus Design

Figure 2-1 shows a schematic of the external fixture for the collinear crystals that was machined from aluminum plates on standoffs of the same. Each crystal was positioned in an individual Helmholtz coil (where the radius r of wire coil is equal to the separation between the two) wound in a consistent direction around plastic spacers with $N = 50$ turns of wire capable of carrying i current. These were connected to 330 μF capacitors capable of discharging at 450V voltage over approximately 500 ms, charged by two Hewlett-Packard power supplies in series. A schematic of the circuitry

is shown in Appendix A.

Using a standard equation for a Helmholtz coil:

$$B = \frac{N\mu_0 i}{\frac{5}{4}r^{\frac{3}{2}}} \tag{2.1}$$

the maximum applied field along the center axis of the coil should have been 8.5 kOe, only slightly less than the theoretical saturation magnetization of Ni_2MnGa of 8.7 kGa. However, calibration with a Bell Model 9200 Gauss probe showed a maximum of only 4.7 kOe, adequate to overcome the blocking stress of the crystals but probably reduced in part due to eddy currents in the standoffs.

During initial trials, the single-crystal laminates were fixed in machined acrylic endpieces that were free to slide in one dimension along parallel brass runners. The crystals were stabilized by a layer of circuit board to prevent buckling as a response to compressive stress from the other crystal. PTFE tape was wrapped around the support board to avoid pinning any of the twin boundaries by an external application of adhesive.

Secondary trials with cut crystals made use of an improved single-runner system and a stiffer plastic for the endpieces and center force-transferrence piece. In all cases one of the pair would begin the trial in a compressed state, with the magnetic easy axis aligned orthogonal to the direction of the applied field, and the other would begin fully elongated, with the magnetic easy axis parallel to the field.

Cyclic magnetic actuation of the crystals was carried out by alternately actuating one then the other sample, recording the strain or displacements with a calibrated eddy current sensor the position of a marker piece of iron in order to capture the position of the midpoint between the crystals relative to the external frame. Initial and final lengths were measured, and engineering strains ($\Delta L/L_0$) calculated.

A four-point resistance probe was constructed to measure the change in resistivity with actuation by means of a Prema 6001 four-terminal digital multimeter. This was to ascertain whether there is an appreciable (i.e., not simply geometric) change in the resistance due to the reorientation of the crystal lattice. This property could later

be used as an indirect measure of the degree of actuation of the twin boundaries. The data for the laminate crystals and the TL8 samples were taken at 21 and 22°C, respectively.

Torque magnetometry was conducted on Digital Measurement Systems equipment using EasyVSM software. The applied field was 100 Oe after a calibration run at zero field, and the sample was oriented so the long direction was parallel to zero degrees. Such a small applied field was chosen so as not to decouple the magnetization M from the c-axis of the crystal lattice.

Chapter 3

Results

Data calculated from analytical experiments are presented here in addition to data collected via the custom apparatus.

3.1 Crystal Characterization

Analytical measurements were collected in order to confirm the suitability of the crystals for the experiment.

3.1.1 Torque Magnetometry

Torque magnetometry was performed in order to estimate the values of the magnetocrystalline and shape anisotropies of the crystals, K_u and K_s respectively. It was predicted that the K_u would be large so that the magnetization would stay coupled to the c-axis of each variant, forcing the crystal to respond to a field orthogonal to the easy axis by rearranging the crystal structure and not by rotating the magnetization.

Since the compositions of the Adaptamat laminate crystals are similar and the microstructures are the remnant of the same growth conditions, the values of K_u were assumed to be equal. This assumption is partly justified on the grounds that an order of magnitude estimate of the value of the magnetostatic energy confirms that it is large relative to the chemical driving force of the atomic interactions [6].

If the applied field $\vec{H}_{app} \ll \frac{2K_u}{M_s}$ with M_s the saturation magnetization, the magnetization can be assumed to be strongly coupled to the easy axis of the crystal. K_s and K_u can be calculated using the approximation that when $\vec{H}_{app} \parallel K_s$, the torque $T \sim K_u + K_s$, because of the constructive effects of the easy crystalline direction and the easy magnetization axis. By the same logic it is apparent that $\vec{H}_{app} \perp K_s$ implies $T \sim K_u - K_s$. This assumes that the field applied by the magnetometer (100 Oe) is not strong enough to decouple the magnetization from the shape anisotropy, which is in line with the long direction of the sample.

As can be seen in Figure 3-1, the torque at 0 and 180° is 550 dyne-cm, and at 90 and 270° from where the long direction of the sample was aligned with the applied field, the torque is -1800 dyne-cm. Solving the equations above and dividing by the sample volume yields a K_u in the laminate crystals of -3125 dyne-cm and a K_s of 5875 dyne-cm.

3.1.2 Vibrating Sample Magnetometry

VSM testing was conducted in order to confirm that the martensitic transition temperature for the crystals was above the operating temperature ($T_M > T_{room}$). The Curie temperature, or the temperature above which the sample ceases to be ferromagnetic and instead becomes paramagnetic was determined for future comparison of samples with differing compositions.

The Curie temperature T_C is calculated using the order parameter S=M of the magnetization versus temperature curve near T_C,

$$M_S{}^2 \sim S^2 = \frac{3(T_C - T)}{T_C} \tag{3.1}$$

and is found to be between 80 and 90°C for each of the TL8 samples, well above any reasonable operating temperature, as can be seen graphically in the representative plot in Figure 3-2

The martensitic transition temperature T_M is by definition, because there is in actuality a small range of temperatures between which the martensite phase is starting

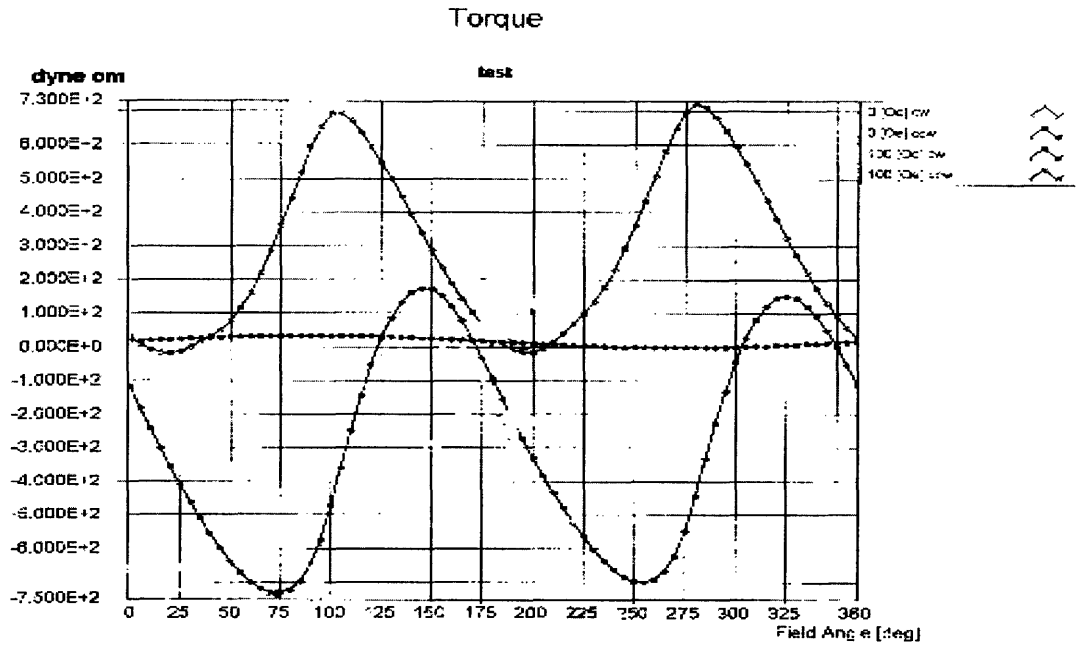

Figure 3-1: Torque magnetometry data from a representative laminate crystal. The applied field of 100 Oe was assumed to be too weak to decouple the magnetization M from the c-axis of the crystal lattice.

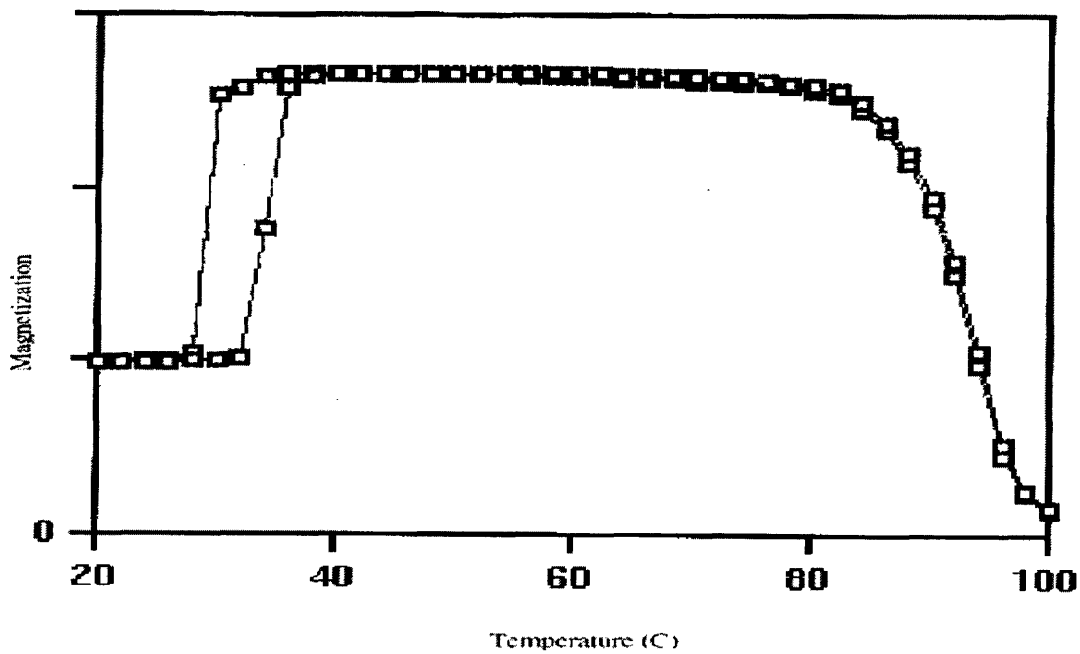

Figure 3-2: VSM plot of magnetization versus temperature showing T_M and T_C. T_M is where the magnetization rises sharply with a slight temperature increase as austenite grows to be the primary phase. T_C is the temperature at which the magnetic moments are no longer as strongly aligned, resulting in a decrease in magnetization.

to grow and has become the primary phase. In the samples cut from the TL8 bulk crystal, T_M was between 30 and 33°C, also above any reasonable operating temperature given the frequency with which the samples are actuated and the energy they must dissipate in response.

3.1.3 Resistance

Resistivities of several available crystals are shown in Table 3.1, showing both a dependence on composition and on variant alignment. Laminate 2-0 showed greater than 12% increase between the resistivity with the current normal to the alignment of the easy axis and that of the current parallel to the orientation of the variant. This large difference is not mirrored by the values calculated for the TL8 samples, which showed at most a 4.2% change.

3.2 Pulse-Field Testing

Table 3.2 shows representative data of cycles where the samples present were the laminate crystals. Each row represents a single trial with a left and right sample comprising the pair. Table 3.3 shows measured and calculated values from TL8 testing. The maximum reset strain observed in the Adaptamat laminates was 1.4%, and 2.8% in the TL8 samples.

Laminate crystals showed an absolute elongation or compression peaking at approximately 0.3 mm where the TL8 samples displaced the midpoint of the apparatus a maximum of aroun 0.4 mm.

3.2.1 Apparatus Improvements

Between the trials with the Adaptamat laminates and those with the samples from Ames National Laboratories, the apparatus was improved as illuminated in the previous chapter. Other changes and possible considerations included mounting the

Sample	Orientation	ρ [Ω -mm]	Anisotropy [%]
TL8-2B	$\perp$	13.66	0.4
TL8-2B	$\parallel$	13.72	
TL8-4B	$\perp$	13.55	4
TL8-4B	$\parallel$	13.01	
A2-0	$\parallel$	15.39	12.9
A2-0	$\perp$	17.68	
A3-1	$\parallel$	14.56	6.8
A3-1	$\perp$	15.63	
A3-2	$\parallel$	14.09	5.0
A3-2	$\perp$	14.82	

Table 3.1: Resistance R was measured with the sensor leads of the four-point setup separated by a distance L =2.59 mm. Orientation is quoted with respect to the magnetic easy axis of the primary variant relative to the applied current direction. Resistivity ρ was calculated using the measured cross-sectional area: $\rho = \frac{RA_{XS}}{L}$.

Left Sample	L_0 [mm]	L_1 [mm]	ϵ [%]	Right Sample	L_0 [mm]	L_1 [mm]	ϵ [%]
A2-0	19.40	19.60	1.03	A3-2	19.62	19.48	-0.72
A2-0	19.47	19.41	-0.31	A3-1	19.76	19.82	0.30
A3-1	19.78	20.05	1.37	A2-0	20.33	20.04	-1.43

Table 3.2: The maximum repeatable reset strain exhibited is 1.4% on each laminate sample, due to a combination of a lossy apparatus and skewed endfaces, resulting in unevenly transferred stresses from the extension of the crystals.

Left Sample	L_0 [mm]	L_1 [mm]	ϵ [%]	Right Sample	L_0 [mm]	L_1 [mm]	ϵ [%]
TL8-2B	19.13	19.26	0.67	TL8-4B	13.62	13.45	1.25
2B	19.06	19.44	1.99	4B	13.58	13.20	2.80
2B	19.90	19.71	0.95	4B	12.94	13.12	1.39

Table 3.3: The TL8 samples showed a maximum reset strain of 2.8%, or a total change in length of 0.38 mm. The improvement is likely a result of an improved force transferrence centerpiece and a more compact cross-sectional geometry in the cut crystals.

crystal holders on ball joints in order to allow imperfectly parallel endfaces to transfer the forces from the crystal elongation, although this was eventually omitted due to complexity.

A stiffer plastic was used to make the center force-transferrence piece and end cups in later tests. A single-runner system was also devised to circumvent any possible losses from moving the centerpiece on slightly skewed tracks.

Chapter 4

Discussion

Torque and VSM measurements confirmed the suitability of the temperature range and magnetic anisotropy value of all the crystals for this experiment, as expected. The fact that there is a change in resistivity with lattice alignment leads to interesting possibilities for indirect measurement of the position of twin boundaries in the future, although this was not explored in the current experiments. Further work is expected to clarify the discrepancies in the differences between the orthogonal and parallel resistivities among the different samples.

In trials with both sets of crystals, a possible source of energy loss that could result in a smaller strain was a slight skew in the end faces. When aligned, the elongated crystal would experience the same compressive reset force from the extension of the first sample but over a smaller contact area. This would make the crystal being compressed appear much stiffer than its calculated value, and take more energy to compress. In addition, having the end face be at an angle less than perpendicular would result in a lower resolved stress on the twin boundaries, making the driving pressure less.

It has also been postulated [8] that small MnO precipitates might pin twin boundaries, hindering their field-induced motion and reducing the overall strain in the sample. Further calculations of the total available energy must be completed in order to compare the expected values of the energy losses in the system with the exhibited strain in the current crystals. Annealing of the crystals in reducing or oxidizing

atmospheres would possibly test this hypothesis.

In original tests with the single crystal laminates, there was doubt as to the extent of the field-induced effect when compared with errors in measurement due to, for example, compression of the crystals during manual setup by overtightening the set screws. For that configuration of the apparatus, there was too much tolerance in the system for crystals of varying sizes, possibly allowing some 'wiggle-room' for each crystal to extend into space without encountering a reactionary force. This was overcome by running through a dummy cycle of actuation and measuring the engineering strain relative to the length after the dummy cycle. In this way, both crystals were at minimum as long as necessary to touch each side of the holders.

The second round of testing certainly benefitted from early planning to only work with one pair of crystals, circumventing any need for adjustability in the runner setup. The crystals were able to sit in precisely-machined end cups and extend against a stiffer plastic to ensure that their sub-millimeter extension would not be absorbed by elasticity in the holder. In addition, the cut crystals had a cross-section that more closely approximated a square, which is a more compact shape for transferring force efficiently.

Some doubt has also been expressed regarding whether the field-induced elongation of the crystals is in fact due to magnetically-driven twin boundary motion. The counterpossibility is that instead of a field-driven growth in the volume fraction of the magnetically favored variant, the crystal responds to $\vec{H}_{app}$ by torquing, and its elongation is a result of the mechanical reaction stress from the constraining holder. While no evidence was presented here to conclusively deny that hypothesis, Tickle and James [3] claim to have confirmed the existence of field-induced twin boundary motion by using polarized optical microscopy.

Chapter 5

Conclusions and Future Work

A significant reset strain was shown to be possible in pairs of FSMA crystals. Detailed energy calculations must be accounted for before any further tests are undertaken in order to compare the available work in an actuated crystal to its extension when perfectly unconstrained. Twin boundary motion is thermodynamically irreversible and inherently dissipative, and it is unclear the extent to which excess energy remains after actuation. The amount of work available after conversion from field energy will be small compared to the amount required for a simple elongation of the crystal by structural reorientation.

In future systems it would also be beneficial to have a small load cell in series with the crystals to measure the stresses as they happen, and not just their effects. It will also be beneficial to have a more complete record of the microstructures as a funciton of the composition and growth processes, in order to better predict whether a crystal will exhibit active twins.

Appendix A

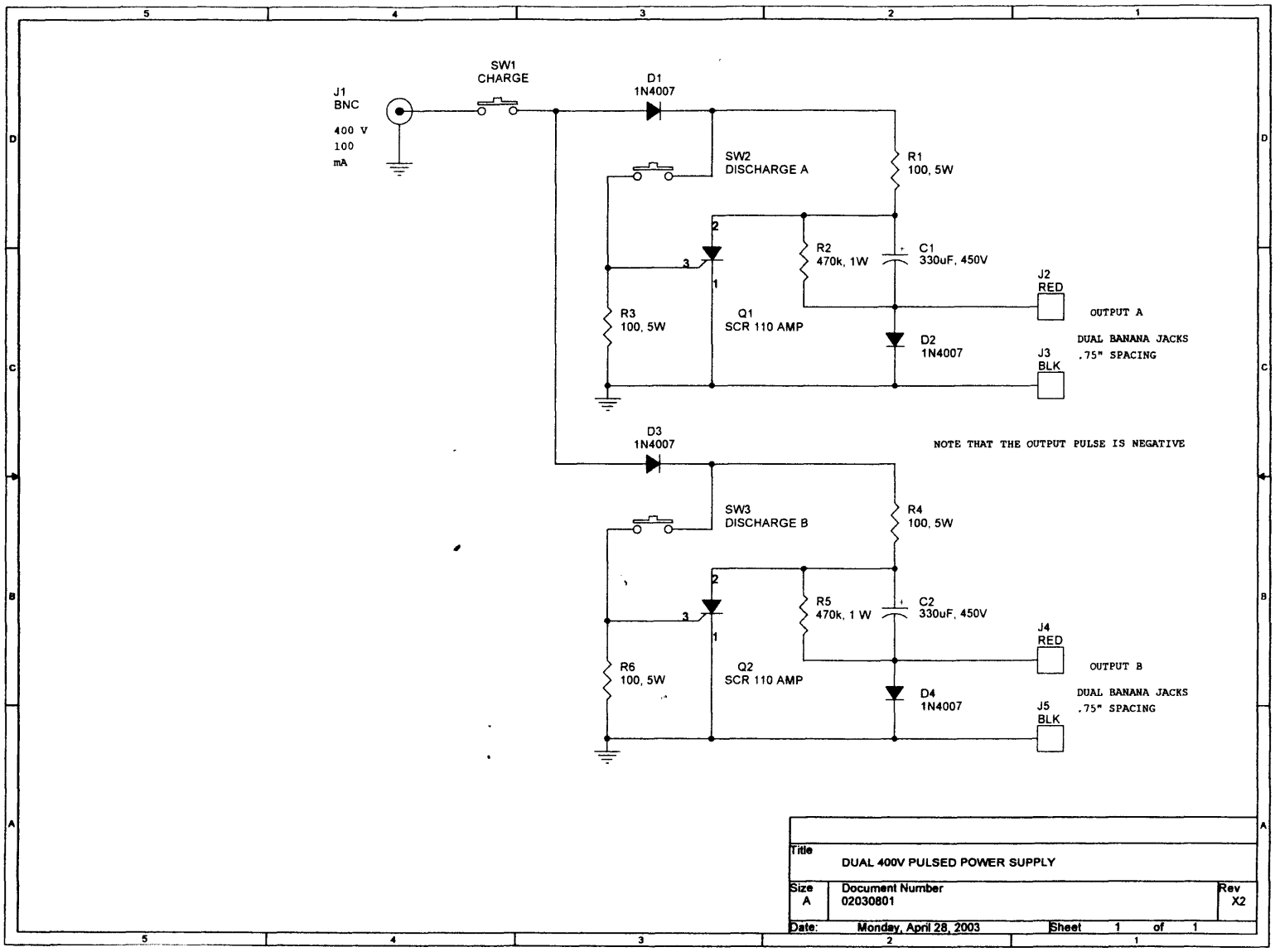

Figure A-1: Schematic of dual circuit for capacitor-driven field actuation

Bibliography

[1] Vassiliev, AN, *Magnetically Driven Shape Memory Alloys*, J Magnetism and Magnetic Mats, vol. 242-245, pp. 66-67, (2001).

[2] R.C. O'Handley, S.J. Murray, M. Marioni, H. Neumbach, S.M. Allen, *Phenomenology of Giant Magnetic-Field Induced Strain in Ferromagnetic Shape Memory Materials*, J Applied Physics, (1999).

[3] *Magnetic and magnetomechanical properties of* Ni_2MnGa, R. Tickle and R.D. James, J Magnetism and Magnetic Mats, vol 195 (1999), pp.627-638.

[4] A. Sozinov, A.A. Likhachev, N. Lanska and K. Ullakko, *J. Appl. Phys.* **80**, 10 (2002), 1746.

[5] *Vibration damping in Ni-Mn-Ga-polymer composites*, J Feuchtwanger, R.H. Ivester, C.A. Jenkins, R.C. O'Handley, S.M. Allen. International Conference on Martensitic Transitions, June 2002.

[6] Murray, S.J. PhD thesis. 2001.

[7] C.P. Henry, D. Bono, J. Feuchtwanger, S.M. Allen, R.C. O'Handley, *J. Appl. Phys.* **91**, 10 pt. 2, 2002, 7810.

[8] *Magnetic domain structure in* $Ni_{53.6}Mn_{23.4}Ga_{23.0}$ *shape memory alloy films studied by electron holography and Lorentz microscopy*, Y Murakami, D Shindo, M Suzuki, M Ontsuka, K Itayaki, Acta Materiala, vol 51, issue 2, (2003), pp. 485-94.

[9] Huang, W., *On the selection of shape memory alloys for actuators*, Materials and Design, vol. 23, pp. 11-19, Feb 2002.

[10] 'What Characteristics Have FSMAs and Electroactive Materials Shown,' http://web.mit.edu/~bobohand/www/gerver/www/fsma/a/index.html. Accessed 23rd March, 2003.